3D seismic study of a ductile shear zone from laboratory and petrofabric data (Saint Barthélémy Massif, Northern Pyrenees, France)

Guilhem Barruol, David Mainprice, Hartmut Kern, Michel de Saint Blanquat, Patrick Compte

▶ **To cite this version:**

Guilhem Barruol, David Mainprice, Hartmut Kern, Michel de Saint Blanquat, Patrick Compte. 3D seismic study of a ductile shear zone from laboratory and petrofabric data (Saint Barthélémy Massif, Northern Pyrenees, France). Terra Nova, 1992, 4, pp.63 - 76. 10.1111/j.1365-3121.1992.tb00451.x . hal-01389722

HAL Id: hal-01389722
https://hal.univ-reunion.fr/hal-01389722v1

Submitted on 29 Oct 2016

HAL is a multi-disciplinary open access archive for the deposit and dissemination of scientific research documents, whether they are published or not. The documents may come from teaching and research institutions in France or abroad, or from public or private research centers.

L'archive ouverte pluridisciplinaire **HAL**, est destinée au dépôt et à la diffusion de documents scientifiques de niveau recherche, publiés ou non, émanant des établissements d'enseignement et de recherche français ou étrangers, des laboratoires publics ou privés.

3D seismic study of a ductile shear zone from laboratory and petrofabric data (Saint Barthélémy Massif, Northern Pyrénées, France)

Guilhem Barruol*, David Mainprice*, Hartmut Kern†, Michel de Saint Blanquat‡[1] and Patrick Compte§[2]

**Laboratoire Tectonophysique, Université Montpellier II, 34095 Montpellier cedex 5, France; †Mineralogisch-Petrographisches Institut, Olshausenstr. 40, 2300 Kiel, Germany; ‡Laboratoire de Tectonique, Université Montpellier II, 34095 Montpellier cedex 5, France; §Compagnie Générale de Géophysique, 1 rue L. Migaud, 91302 Massy cedex, France*

ABSTRACT

In order to constrain interpretations of seismic reflection records more effectively, the seismic properties of a middle crustal section exposed in the Saint Barthélémy Massif have been determined. The massif, transected by a 200 m thick shear zone has been systematically sampled for density measurements and modal analysis has been performed in order to define the spatial variations of physical properties. Seismic velocities (V_p, V_s, shear wave birefringence), have been measured on five representative samples to 600 MPa and 600°C simultaneously in the three structural directions (X, Y and Z). For two samples, the experimental data have been compared with calculated values, based on petrofabric analyses. The Lattice Preferred Orientation (LPO) is determined using universal stage, electron channelling microscopy and neutron diffraction goniometry. Using the experimental and calculated velocity data, we establish a lateral homogeneous anisotropic model.

Terra Nova, **4**, 63–76

INTRODUCTION

Deep seismic profiling of the lower continental crust has revealed many strong reflections. Up to now, their origins have been poorly understood. Low-angle reflections are often interpreted as ductile shear zones, e.g. COCORP and the Brevard Fault (Cook *et al.*, 1979), ECORS-Alps and the Penninic front (Nicolas *et al.*, 1990), ECORS-Pyrenees and the Variscan thrust (Choukroune *et al.*, 1989). Laboratory seismic measurements have shown that preferred orientation of anisotropic minerals (in particular phyllosilicates), may have a significant effect on seismic rock properties (e.g. Fountain *et al.*, 1984; Jones and Nur, 1984). The gently dipping reflections observed across geological structures such as the Brevard mylonite zone (Christensen and Szymanski, 1988) and the Kettle river mylonite zone (McDonough and Fountain, 1988) have been directly related to a large volume of oriented biotite minerals in ductile shear zones. Recently, Kern and Wenk (1990) have shown that, at constant bulk composition, seismic anisotropy in mylonites increases significantly with the amount of strain, i.e. with the degree of preferred Lattice Orientation (LPO) of phyllosilicates.

The aim of this study is to understand better the seismic response of a middle crust ductile shear zone. Different but complementary methods have been used for determinations of seismic properties of rocks: laboratory velocity measurements and velocity calculation based on petrofabric data.

The samples were collected from a geological structure exposed in the Saint Barthélémy Massif (Northern Pyrénées) representing a middle crustal section transected by a thick ductile shear zone. Its structure, composition and geometry was already well constrained by previous studies (Passchier, 1982; Saint Blanquat, 1989).

We have chosen five samples representing the main lithological units for the laboratory measurements and for two of these samples the seismic velocities have been calculated from the elastic constants of the constituent minerals and their LPO. Using a combination of experimentally and petrofabric-derived (cross-checked) rock elastic constants, we have modelled the seismic response of this exposed structure. The synthetic seismograms are the result of a calculation taking into account the 21 elastic constants characterizing the elastic properties of each unit.

GEOLOGICAL SETTING

Lithology of the Saint Barthélémy Massif

The Saint Bathélémy Massif (Passchier, 1982; Saint Blanquat, 1989) is located in the North Pyrenean Zone (Fig. 1a). It is separated from the Variscan Axial Zone by a major crustal structure, the North Pyrenean Fault. The crustal section consists of the following bottom-to-top sequence (Fig. 1b):

(i) a paragneissic formation (2 km thick) containing small lenses of marble and amphibolite. The gneisses have been metamorphosed under LP–HT granulite facies conditions (750±50°C and 500±50 MPa) at late Variscan time (*c.* 300 Ma, Delaperrière, pers. comm.). The main penetrative deformation of this basement is interpreted as

[1]Present address: Laboratoire pétrophysique et téctonique, Université Paul Sabatier, 3214090 Toulouse, France.

[2]Present address: IFP, BP 311, 92506 Rueil Malmaison, France.

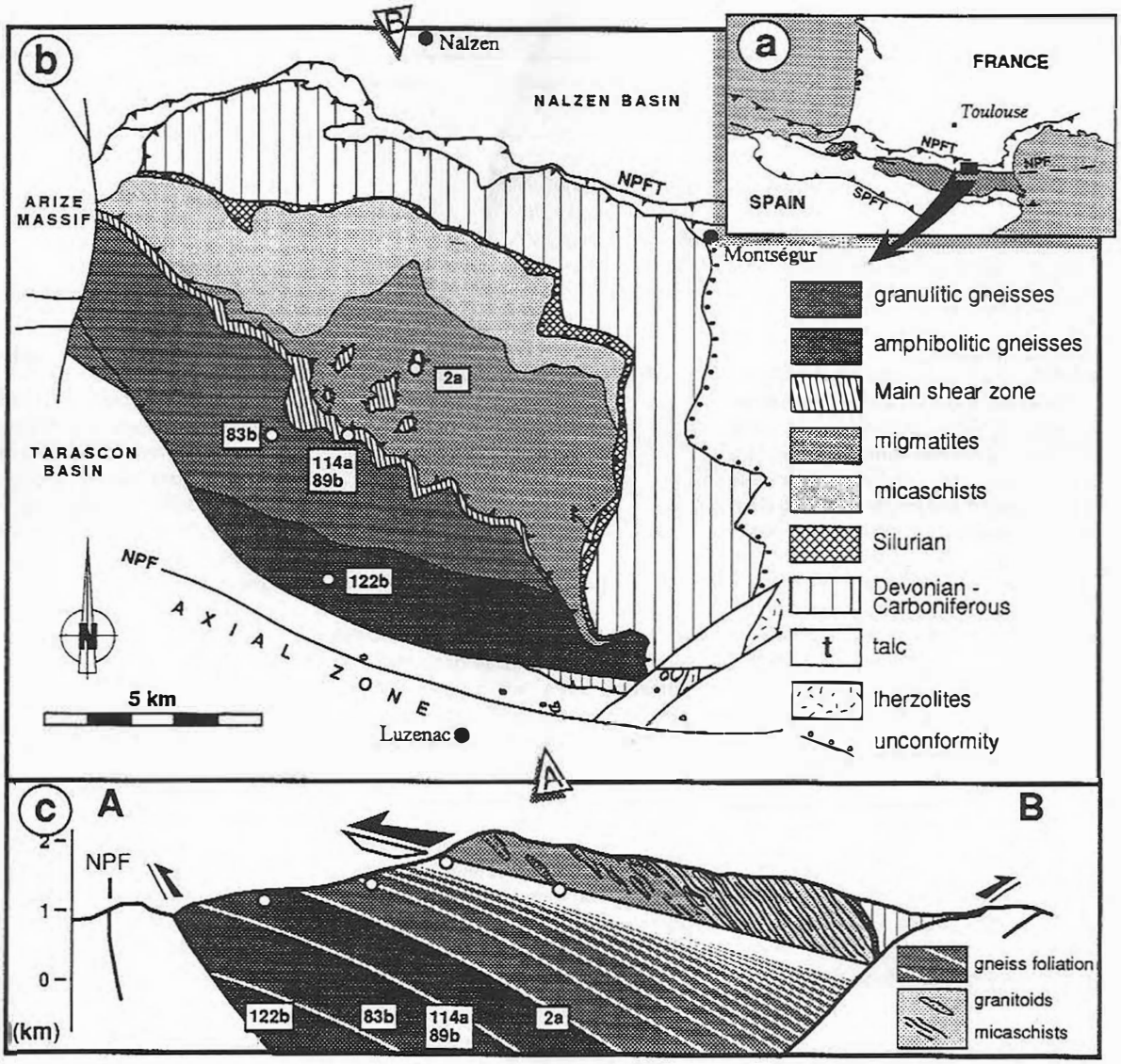

Fig. 1. *(a) Location map of the Saint Barthélémy (NPF: North Pyrenean Fault, NPTF: North Pyrenean Frontal Thrust, SPTF: South Pyrenean Frontal Thrust). (b) Schematic geological map of the massif, with sample locations (from Saint Blanquat, 1989). (c) Schematic cross section (the sample locations are projected onto the cross section).*

having resulted from a progressive extensional event which started with granulitic metamorphism (Saint Blanquat, 1990).

(ii) a low angle ductile shear zone, 50–200 m thick, was initiated during the latest stages of the ductile deformation ($T \approx 450$°C). It is composed of several anastomosing quartzo-feldspathic mylonites and mylonitized carbonate layers enveloped by a 1–5 m thick ultramylonite band.

(iii) migmatites and micaschists (2 km thick) derived from lower Paleozoic series and intruded by granodioritic and leucogranitic sills.

(iv) an Upper Paleozoic series (shales and carbonates).

Structure of the massif

The foliation, both in the hanging wall (migmatites and micaschists) and in the footwall (granulitic and amphibolitic gneisses) of the ductile shear zone, is oriented N100 30°N. A pronounced N–S trending stretching lineation is developed in the shear zone and in the lower unit. The ductile shear zone (Fig. 1c) crosscuts the foliation in the bordering rocks at a small angle (15°). The strain increases markedly from the granulites to the ultramylonites. The overlying migmatites are undeformed. The total outcropping thickness of the ductile deformed zone (including gneisses) is about 2 km.

Table 1. Modal composition and density of the five selected samples

Sample	Rock type	Density ($g cm^{-3}$)	Modal analysis
SB2a	Phyllonite	2.83	100% Phyllosilicates
SB89b	Biotite rich ultramylonite	2.79	45% Biotite, 25% feldspars, 30% quartz
SB114A	Ultramylonitic quartzite	2.58	100% Quartz
SB83	Amphibolitic gneiss	2.65	35% Quartz, 15% biot., 28% micr., 18% plag., 2% sill, 2% garnet
Sb122b	Acid granulite	2.93	45% Quartz, 22% felds., 15% garnet, 8% biot., 5% sill, 5% opx

Rock samples

115 samples were collected from two N–S cross sections transecting the whole massif. Bulk densities were measured and lie within a narrow range of 2.6–2.8 g cm^{-3} indicating a relatively homogeneous, silica rich crustal section. The modal compositions of 40 of the samples were measured by an image analysis technique (Allard and Sotin, 1988). Based on the modal composition and the density measurements we have selected 5 representative samples, 3 from the shear zone (SB2a, SB89b, SB114a) and 2 from the lower unit (SB83, SB122b). The upper unit composed of migmatites, leucogranites and micaschists, has been considered, at a first approximation, to be isotropic due to the extreme variability of lithologies and structures. Localities of these samples are indicated in the schematic geological map (Fig. 1b) and projected on a cross section plane (Fig. 1c). The sample modal compositions and densities are listed in Table 1.

LABORATORY SEISMIC MEASUREMENTS

Method

The velocity measurements at PT conditions were carried out in a cubic pressure apparatus at the Mineralogisch-Petrographisches Institut, Kiel (Germany) using the pulse-transmission technique. The method allows simultaneous measurements of P and S-wave velocities in the three structural directions (X, Y and Z) of the cube-shaped specimens (Kern, 1982). Velocities were generally measured as a function of pressure (up to 600 MPa) and as a function of temperature (up to 600°C) at a constant confining pressure of 600 MPa. For the determination of acoustic birefringence we used two sets of shear wave transducers with perpendicular polarization directions. S-waves were polarized in the XY, XZ and YZ planes. Assuming the fastest and the slowest velocities were generally measured parallel and normal to the foliation plane respectively, we determined the velocity anisotropy. The velocities of the two perpendicularly polarized shear waves propagating in the X, Y and Z directions allow in addition the calculation of acoustic birefringence. In the following text, V_{sij} represents the velocity of a shear wave propagating in the ij plane, in the j direction.

P-wave measurements

At low pressure conditions, average values increase rapidly with increasing pressure (Fig. 2), reflecting the closure of microcracks. Above 200 MPa the curves become linear and represent the intrinsic elastic properties of the

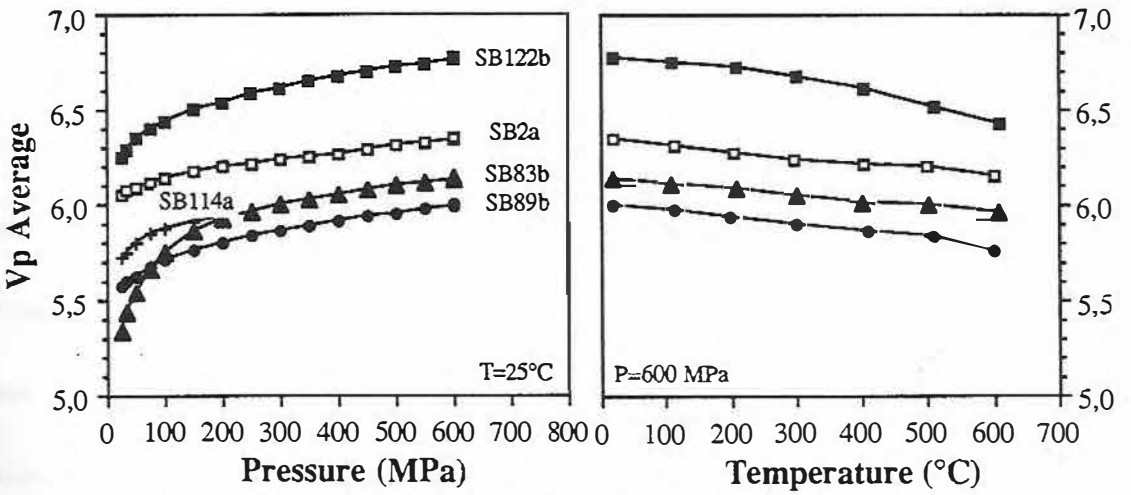

Fig. 2. *Average measured P-wave velocities from the three structural directions of the five samples as a function of pressure at room temperature (left) and as a function of temperature at 600 MPa confining pressure. The sample SB114a has been measured only up to 200 MPa and is absent on the right-hand diagram.*

samples. The P-wave velocities are not strongly influenced by the pressure increase above 200 MPa. For the phyllonite SB2a, for example, a pressure increase of 400 MPa generates a V_p increase of about 0.15 km s^{-1}. At 600 MPa a temperature increase results in a slight linear decrease of velocities. The derivatives of seismic velocities (Table 2) refer to the (quasi) linear slopes of the velocity-pressure and velocity-temperature relation, respectively between 200–600 MPa and 20–500°C. The 600 MPa (room temperature) P-wave velocities are in a range of 5.8 and 6.8 km s^{-1}, which was found to be typical for acidic rocks of low (phyllonite, mylonite) and high (granulite) metamorphic grade (Kern and Schenk, 1988; Kern and Wenk, 1990).

The studied samples exhibit significant velocity anisotropy. Slowest velocities were generally measured normal to the foliation plane, i.e. parallel to Z (Table 2). Anisotropies ($A\% = 100\ (V_{max}-V_{min})/V_{max}$) vary between 2% (gneiss SB 83b) and 16% (phyllonite SB2a) at 200 MPa. At and above this pressure, where most of the cracks are closed, anisotropy is mainly caused by crystallographic and shape-preferred orientation of minerals (texture). In the very low pressure range, however, oriented microcracks make a major contribution to velocity anisotropy producing the highest anisotropy values. The present results also confirm earlier observations (Barruol, 1988; Mainprice and Nicolas, 1989) that anisotropy decreases with the number of mineral species in the rocks (Table 2), and is most pronounced in phyllosilicate rich rocks. The phyllonite SB2a illustrates this phenomenon well: P-wave velocity within the foliation plane is very homogeneous and fast, whereas the slowest is normal to the foliation (Fig. 3 bottom). It displays a strongly transverse isotropy characteristic of textured biotite-rich rocks (see also Kern, 1990). It is important to recognize that apart from the α–β quartz transition, the texture related anisotropy is almost pressure and temperature independent (Kern, 1990).

The quartzite mylonite SB114a displays well the influence of α–β quartz transition on anisotropy. At room temperature, the fast V_p velocity is parallel to the Y structural direction and the slow velocity is parallel to the X direction (Fig. 3 top). With increasing pressure, the anisotropy remains almost constant (about 10%). At 200 MPa, an increase in temperature up to 630°C reveals an important decrease of V_p of almost 1 km s^{-1}. Simultaneously, the properties change from strongly anisotropic (10%) to nearly isotropic (2%). Above the transition, V_p increases markedly by about 2 km s^{-1} and exhibits only a small directional dependence in the β-field (see also Mainprice and Casey, 1990).

S-wave measurements

Pressure and temperature influence on S-wave velocities are qualitatively very similar to P-waves. The difference $\Delta V_s = V_s0 - V_s90$ (see Table 2 for definitions) for each structural direction characterizes the shear wave birefringence. Typical values range fom 0 to 0.3 km s^{-1}. Pressure and temperature derivatives determined from the linear slope of the seismic velocities (Table 2) yield values in agreement with previous determinations (Christensen, 1979; Kern and Richter, 1981).

In elastically anisotropic rocks, shear-wave velocities strongly depend on their polarization directions. Pronounced acoustic birefringences (shear

Table 2. Laboratory velocity measurements summary, for the three structural directions, for the P-waves (velocities, anisotropies, pressure and temperature derivatives) and for the S-waves (velocities, birefringence, pressure and temperature derivatives). The temperature derivatives have not been calculated for sample SB114a due to the non linearity of the curves.

Sample		P-waves		S-waves			Derivatives			
		V_p (km s^{-1})	AV_p %	V_{s0} (km s^{-1})	V_{s90} (km s^{-1})	ΔVS (km s^{-1})	dV/dP ($\times 10^{-4}$ km s^{-1} MPa^{-1})		$-dV/dT°$ ($\times 10^{-4}$ km s^{-1} °C^{-1})	
							P-waves	S-waves	P-waves	S-waves
SB2a	//X	6.60		yx 4.06	zx 3.00	1.06				
	//Y	6.50		xy 4.12	zy 3.03	1.09				
	//Z	5.49	16.8	xz 3.01	yz 3.00	0.01	3.33	1.33	2.83	1.50
SB89b	//X	6.01		yx 3.76	zx 3.38	0.38				
	//Y	5.97		xy 3.81	zy 3.37	0.44				
	//Z	5.42	9.8	xz 3.24	yz 3.27	0.03	5.33	1.16	3.67	1.33
SB114a	//X	5.63		yx 3.83	zx 4.15	0.32				
	//Y	6.24		xy 3.90	zy 4.12	0.22				
	//Z	5.95	9.7	xz 4.13	yz 4.15	0.02	5.50	3.5	?	?
SB83b	//X	5.97		yx 3.57	zx 3.57	0.00				
	//Y	5.93		xy 3.63	zy 3.49	0.14				
	//Z	5.87	1.6	xz 3.49	yz 3.58	0.09	3.33	1.33	2.60	0.50
SB122b	//X	6.82		yx 3.89	zx 3.86	0.03				
	//Y	6.67		xy 3.71	zy 3.60	0.11				
	//Z	6.14	10.1	xz 3.67	yz 3.67	0.00	5.50	1.33	#4.42	#1.71

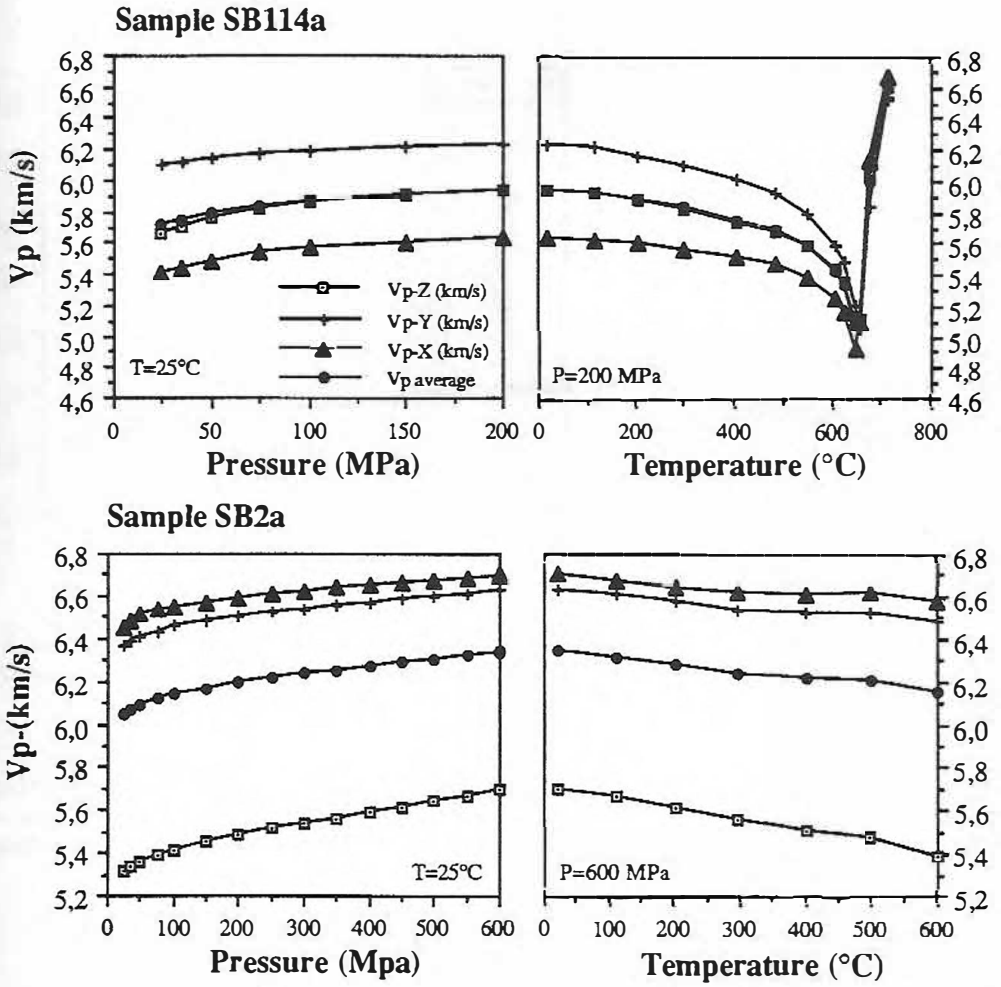

Fig. 3. *Laboratory measurements of V_p for the quartzite SB114a (top) and of the phyllonite SB2a (bottom), with increasing pressure (left) and with increasing temperature (right). The velocities measured in the three structural directions are plotted. The caption is the same for the two samples.*

wave splitting) were observed in the phyllonite and mylonite samples (SB2a, SB89b and SB114a). Birefringence as high as 1 km s^{-1} was observed within the foliation plane (Table 2). Shear wave splitting is closely related to the structural framework. The fast and slow shear-waves are respectively polarized parallel and normal to the foliation. In the phyllonite SB2a, for example (Fig. 4) V_{szy} and V_{syx} are the fastest S-waves because both their propagating directions and their polarization planes are contained in the *XY* plane. In such biotite rich rocks, therefore, S-waves propagating either normal to the foliation or polarized perpendicularly to it have low velocities.

3D seismic properties extrapolated from direct measurements

The technique we used to model the anisotropic seismic properties of our geological object requires the 21 elastic constants for each element of the model, that means we need to extrapolate the velocities (V_p, V_s) measured in the three mutually perpendicular directions (*X*,*Y*,*Z*) to an arbitrary direction. To determine the shape and the axial ratio of the velocity ellipsoid, the Flinn diagram has been used. The ratio V_{px}/V_{py} versus V_{py}/V_{pz} is plotted for each sample (Fig. 5). In an ideal transverse isotropic case, the point would be placed on the $K = 0$ or $K = \infty$ axes (corresponding to pancake-like and cigar-like ellipsoids, respectively). The points representing the three studied samples (SB2a, SB89b and SB122b) fall close to the line $K = 0$ ($K = 0.064$, 0.038 and 0.273, respectively). The *K* values are defined as $K = ((V_{px}/V_{py})-1)/((V_{py}/V_{pz})-1)$. The velocity ellipsoids determined for these three samples are close to the transversely isotropic case ($K = 0$), especially for the two mylonites (SB2a and SB89b). Their elastic constants (Fig. 9) can now be determined for these three samples assuming the symmetry to be transverse isotropic, using the method described in Christensen and Crosson (1968) and in Seront *et al.* (1992). The low V_p aniso-

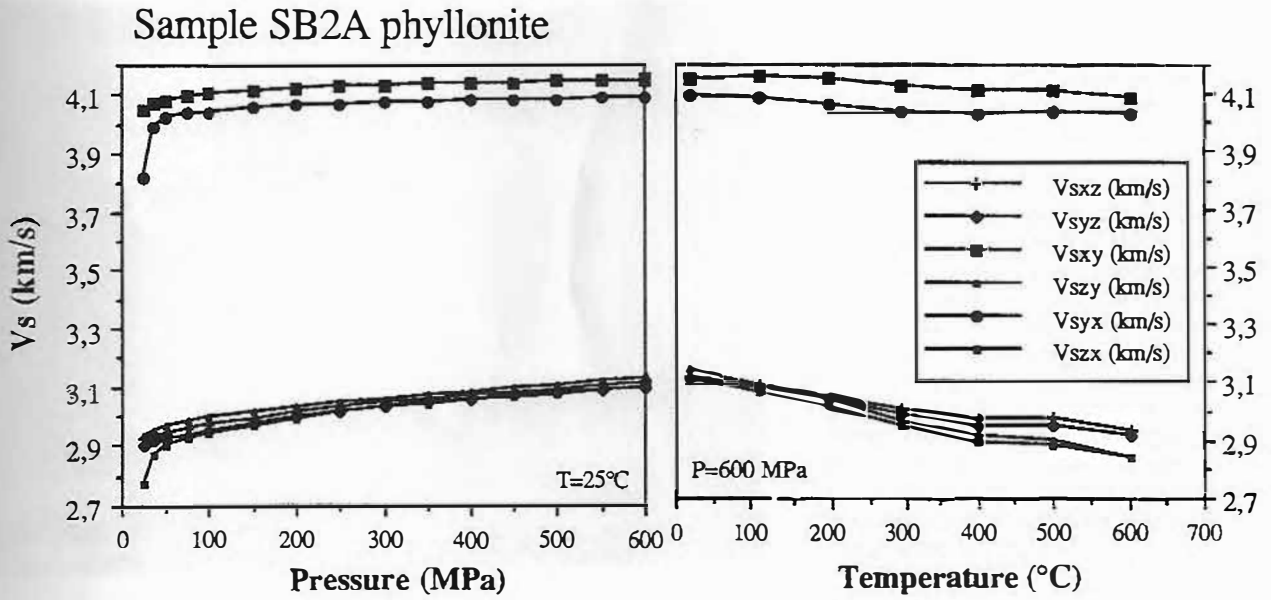

Fig. 4. *S-wave measurements for phyllonite SB2a along the six polarization planes (cf Table 2 for the notion of* V_s*) with increasing pressure (left) and with increasing temperature (right).* V_{sij} *represent a shear wave velocity within the* ij *plane and in the* j *direction.*

tropy (1.4%) of the gneiss SB83 explains why the shape of its velocity ellipsoid is not significant. The quartzite SB114a is close to the line $K = -1$, and cannot be described as a transverse isotropic case.

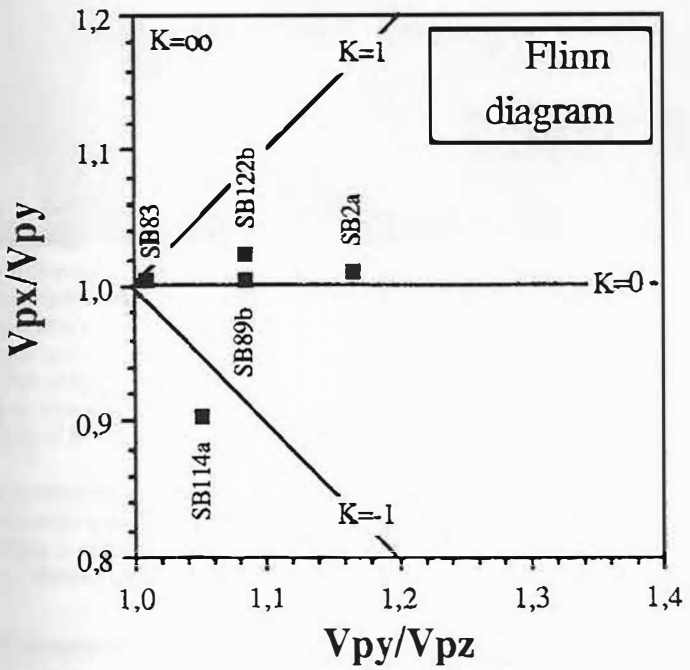

Fig. 5. *Flinn representation of the anisotropy of the laboratory measured P-wave velocities for the five samples. (see text for explanations).*

VELOCITY CALCULATIONS FROM PETROFABRIC DATA

Determination of Lattice Preferred Orientation (texture)

Two specimens (SB114a and SB83b) were selected for the velocity calculations. The microstructures of the specimens are illustrated in Fig. 6.

Pole figures of quartz in sample SB114a were measured by neutron diffraction goniometry. A solid cylinder (10 mm diameter and 20 mm length) of this monomineralic and fine-grained rock (10 μm) provides a good statistical representation of the crystallographic texture. LPO of mineral phases of the gneiss SB83 were obtained either using the universal stage on an optical microscope (biotite) or by scanning electron microscopy (SEM) using the selected area electron channelling pattern (SAECP) method (Quartz, Plagioclase and K-feldspar) (Lloyd *et al.*, 1981). SEM provides a powerful tool for measuring partial textures in polyphase material, in particular for minerals optically difficult to measure (plagioclase) or from which it is impossible to obtain complete crystallographic information (quartz). The SEM determination of the complete crystallographic orientation

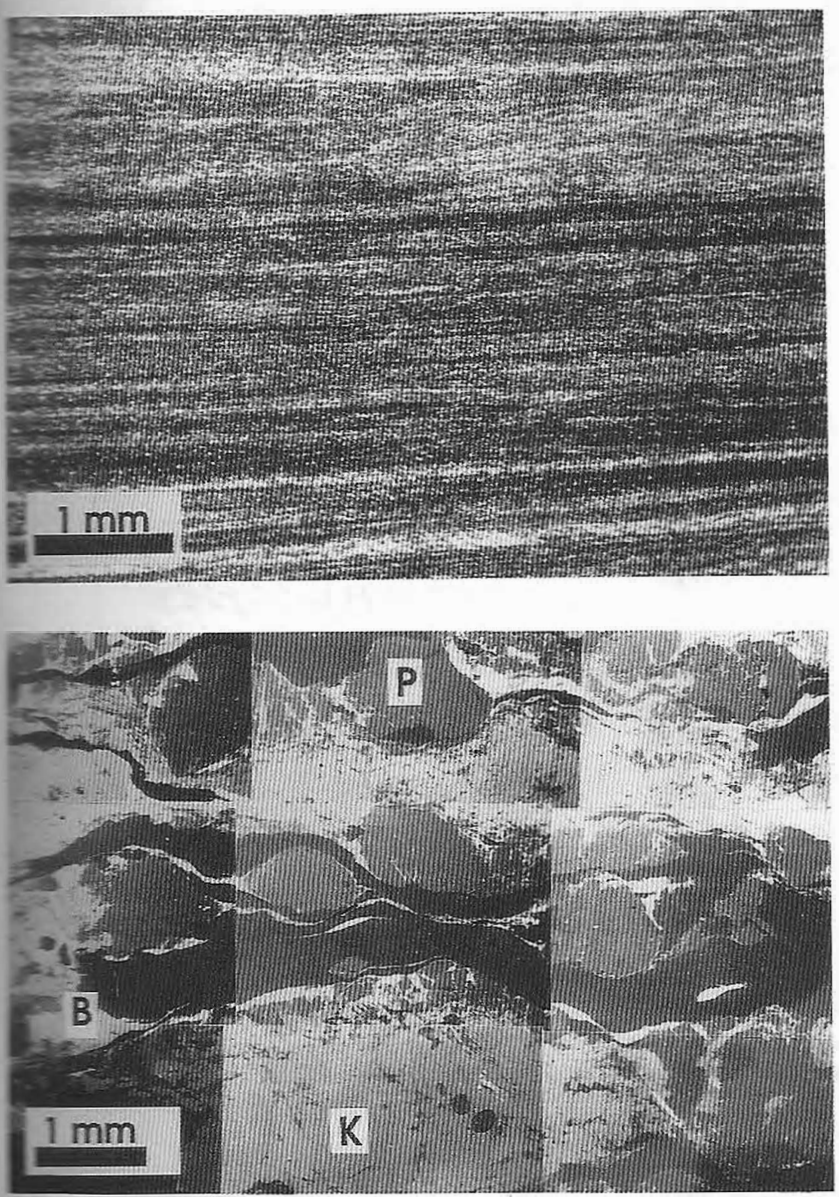

Fig. 6. *Microphotographs of the monomineralic quartzite, optical microscopy, crossed nicols (top) and of the polymineralic gneiss, SEM backscattered image (bottom), both in the XZ plane. The quartzite is very fine grained (10 μm) and strongly textured. In the gneiss, quartz microstructure is typical of plastic deformation. Grains are ribbon shaped and often bent around strain free feldspar porphyroclasts. Despite the intense plastic deformation, quartz grains display no sign of dynamic recrystallization. Q = quartz, K = K-feldspar, P = plagioclase and B = biotite.*

of each grain is obtained by indexing the recorded channelling pattern (Lloyd *et al.* 1987) using a computer program (Schmidt and Olesen, 1989).

Procedure of velocity calculation

The calculation of the three dimensional distribution of elastic seismic velocities (V_p, V_s, shear wave splitting) in an anisotropic polymineralic rock is based on the knowledge of the Lattice Preferred Orientation (LPO or petrofabric) of each mineral species, the volume fraction of each mineral, the crystal densities and the elastic stiffness coefficients. The grain shape preferred orientation is not taken into account in these calculations. The procedure of calculation is described in detail by Crosson and Lin (1971) and Peselnick (1974). Computations were performed using an interactive program (Mainprice, 1990).

The elastic constants of α-quartz single crystal (trigonal) used were those reported by McSkimin *et al.* (1965), and for biotite (monoclinic, pseudohexagonal) we used those recently reported by Vaughan and Guggenheim (1986) for muscovite. The seismic properties of muscovite are very close to those determined by biotite (considered as hexagonal) by Aleksandrov and Ryzhova (1961). The data for feldspars used in these calculations were determined by Aleksandrov *et al.* (1974) for microcline and plagioclase (An29%).

Lattice Preferred Orientation (LPO) and calculated velocity distributions

The lattice preferred orientations of the major minerals constituting sample SB114a (quartzite) and SB83 (gneiss) are documented in Figs 7 and 8, respectively.

In the quartzite SB114a, (Fig. 7 left) the maximum of quartz **a**-axes is close to the lineation and the **c**-axes are grouped in two maxima between the *Y* and *Z* structural axis. The **m**-axes pole figure (not shown) is very similar to the **a**-axes pole figure and the **r**+**z** measured pole figure (not shown) exhibits two maxima between the *Y* and *X* directions, in the foliation plane. The fabric does not exhibit any clear obliquity with respect to the structural frame (*XYZ*). These pole figures could arise from intracrystalline slip mainly on the rhombohedral **r** crystallographic plane, in the [**a**] directions. The pole figures of the polymineralic gneiss SB83 are shown in Fig. 8 (left).

The **Quartz** **c**-axes form a broad girdle in the *YZ* plane, with a maximum close to the *Y* axis. The corresponding **a**-axes scatter around *Y* in the projection plane. This fabric is typical of amphibolite facies metamorphic conditions (Mainprice and Casey, 1990; Schmid and Casey, 1986). The **Biotite** **c**-axes (close to the pole of the main cleavage of the crystal, the (001) plane) form a strong maximum normal to the foliation, with a larger angular spread toward *X* than toward *Y*, mainly due to deflection of the foliation around the feldspars por-

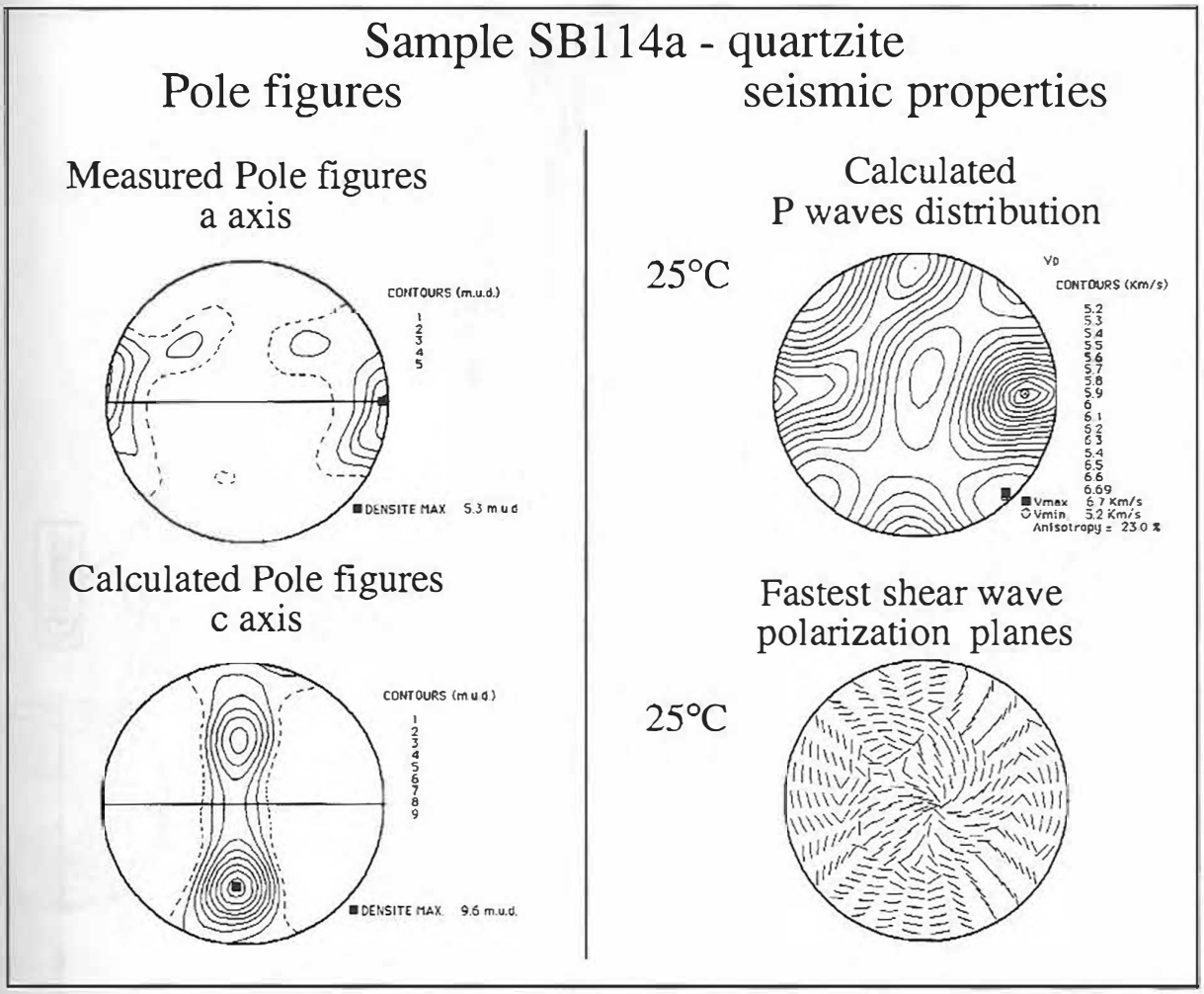

Fig. 7. *Quartzite SB114a: a and c-axes pole figures (left) and some calculated seismic properties from these petrofabrics (P-wave velocity distribution at 25°C and the orientation of the fastest S-wave polarization planes). The equal area projections are in the lower hemisphere, the foliation is EW, normal to the paper and the lineation EW.*

phyroclasts. For seismic properties computation, the a-axis orientation of each biotite grain, has been generated randomly in a plane normal to the pole of the cleavage (c*), assuming biotite to be transverse isotropic. Pole figures of **K-feldspar** and **plagioclase** a-axes and of the +(001) planes do not exhibit any preferred orientation. It should be mentioned, however, that the small number of measured grains may not give a statistical representation of the aggregate.

Figure 7 (right) presents the calculated velocity surfaces of the **monomineralic quartzite SB114a**. The minimum P-wave velocity (V_{pmin}) is close to X and correlates to the a-axes maximum. The a-axis represents the slowest velocity in the quartz single crystal. V_{pmin} parallel to X is in good agreement with experimental measurements (see Table 2). V_{pmax} lies between the X and Z axis and is related to the z crystallographic axis (not shown) which represents the direction of the fastest P-wave in quartz single crystal. The corresponding shear wave properties (V_s and polarization planes) have been calculated and are shown in Figs 9 and 7, respectively. In an anisotropic aggregate shear waves split into two waves with different velocities and polarization directions (Crampin, 1985). The two shear waves V_s1 (fast) and V_s2 (slow) are polarized in mutually perpendicular planes. In equal area projection (Fig. 7), the shear wave polarization is indicated by a little arc segment of a great circle. The arc marks the orientation of the fastest shear wave (s1).

Considering the quartzite specimen in its structural framework, it follows from Fig. 7 (orientation of the polarization planes) and of Fig. 9 (spatial distribution of V_{s1} and V_{s2}) that significant shear wave splitting occurs for S-waves propagating parallel to the foliation plane. The fast shear waves (s1) close to the lineation are polarized normal to the foliation plane, and the corresponding slow shear wave (s2) parallel to it. This is in excellent accordance with the experimental results (see Table 2). On the

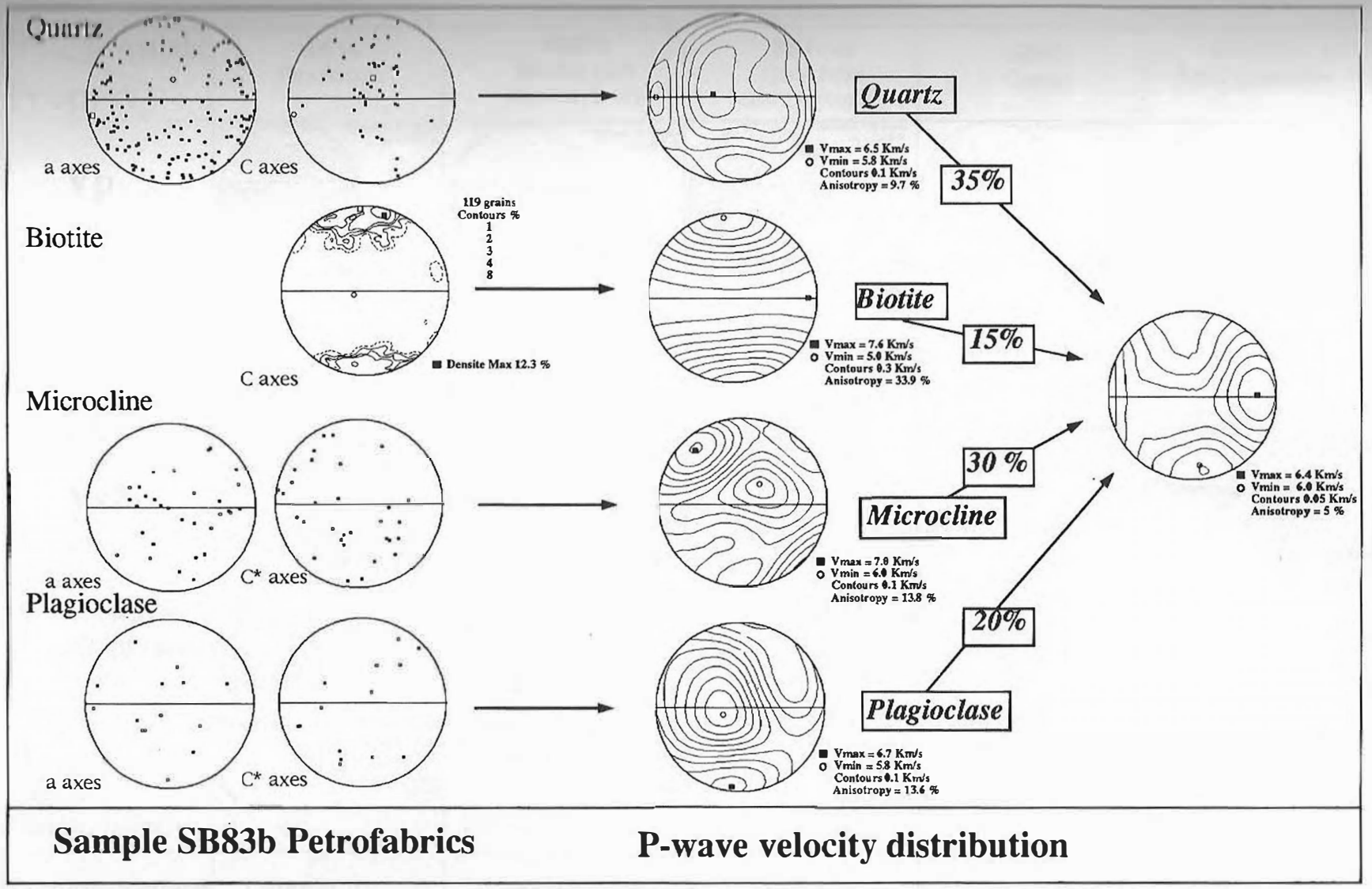

Fig. 8. *Gneiss SB83b: Calculation of the P-wave velocity distribution of a complex aggregate from the knowledge of the preferred orientation of each mineral phase. On the left, preferred orientation of the* **a** *and* **c** *crystallographic axes of quartz, biotite, K-feldspar and plagioclase. In the middle part of the figure are shown the P-wave velocity distributions of each virtual single phased aggregates. The modal composition is used to calculate the* V_p *spatial distribution taking into account each mineral phase in its bulk proportion. The equal area projection characteristics are the same as in Fig. 7.*

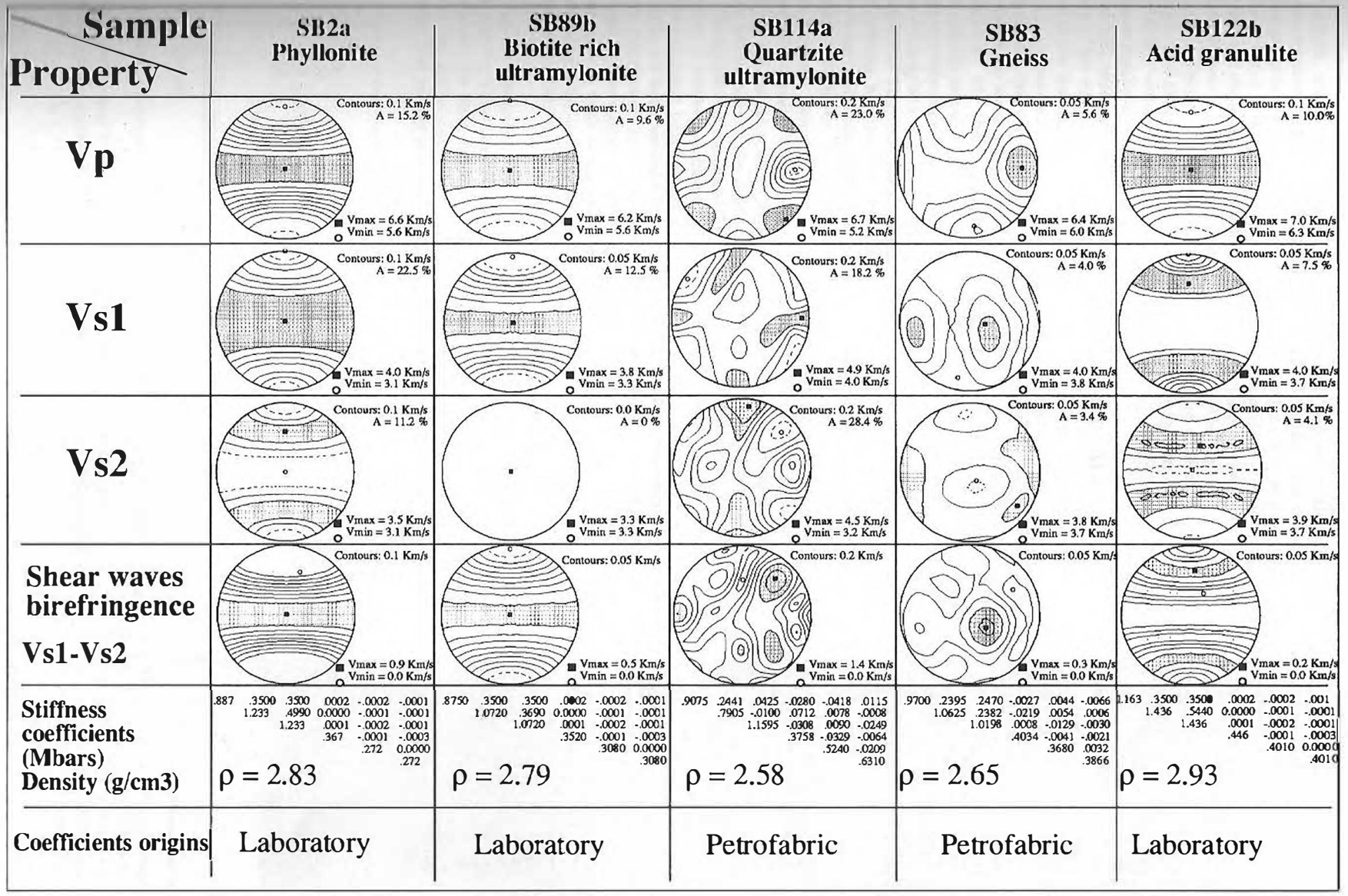

Fig. 9. *Seismic properties of the five samples studied. Shown are the velocity distribution of the P-waves, of the two S-waves (for their significance see text), of the birefringence and the 21 elastic constants controlling the aggregate property (in Mbar). The velocities of the samples SB2a, SB89b and SB122b are laboratory derived. For the samples SB114a and SB83b the velocities are petrofabric derived. The equal area projection characteristics are the same as in Fig. 7.*

other hand, returning the quartzite sample to its crustal setting assuming its foliation is horizontal, and considering a seismic wave propagating upward vertically, the shear waves will split at the lowest interface of the quartzite layer and will propagate with different velocities. The fastest (s1) will propagate vertically within the *XZ* plane, i.e. in a plane parallel to the lineation. The slowest (s2) will propagate vertically too, but in the *YZ* plane, i.e. in a plane normal to the lineation. In real seismic records, measurements of the delay time between the two shear wave arrivals, the shear wave splitting and the orientations of their polarization planes, allows one to extract structural kinematic information. The polarization plane of s1 may be a marker of the lineation, and the magnitude of the shear wave splitting may indicate the combined values of anisotropy and the thickness of the layer.

The velocity distribution of the **polymineralic gneiss SB83** (Fig. 8) is based on the partial textures and the volume percentages of the major minerals. The direction of the fastest P-wave is close to *X* within the foliation plane and the calculated bulk velocity anisotropy is found to be around 5.6%. The velocity distribution in the composite aggregate is dominated by the biotite crystals, due to their strong preferred orientation and the pronounced velocity anisotropy (33.9%) of this mineral species.

In Fig. 10 comparison is made between measured and calculated P-wave velocities in the three structural directions of the gneiss and ultramylonitic quartzite. The results obtained by the two methods compare fairly well. The maximum deviations are around 4%. This small value could be explained by the shape preferred orientation of grains, not taken into account in these calculations. The calculated velocity anisotropies are generally higher than those measured experimentally.

SEISMIC MODELLING

The synthetic seismogram program (DRT4) uses a 3D ray tracing method. It generates seismic traces for three component receivers. The receivers and the source may be in any geometrical disposition, at the surface or at any depth. The geometric model is a parallelepiped divided in homogeneous or heterogeneous layers. Each layer is defined by its physical properties (the density and the 6 by 6 elastic stiffness (C_{ij}) matrix) and by its three dimensional geometry, excepting discontinuities. The program may generate all types of seismic signatures (reflection, transmission or multiples) for P and S-waves but they must be explicitly specified in the input parameters. The ray path in each layer is obtained calculating first the isotropic case and then calculating the pertubation due to three dimensional velocity distribution. The obtained seismic traces are not true amplitude.

Schematically, the algorithm used by DRT4 is the following: the first step is a scan to find the rays joining source and receivers. The second step is a ray tracing including amplitude computation along the selected rays which allows a modelling using the 'Gaussian Beams Technique'. The last step is the computation of the seismic traces.

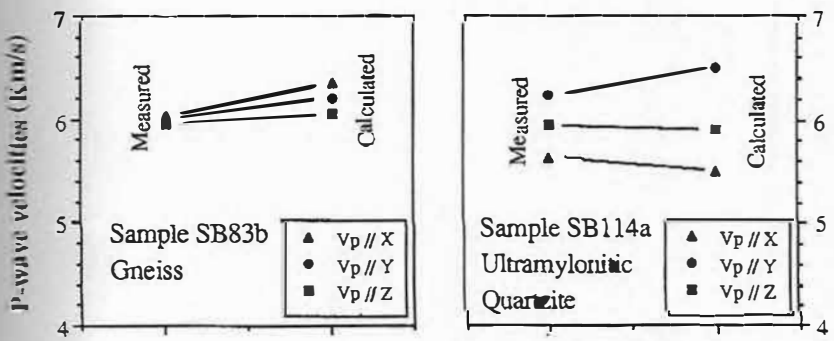

Fig. 10. *Comparison of P-wave velocities measured (in laboratory) and calculated (from petrofabrics) for the samples SB83 (left) and SB114a (right), and for the three structural directions.*

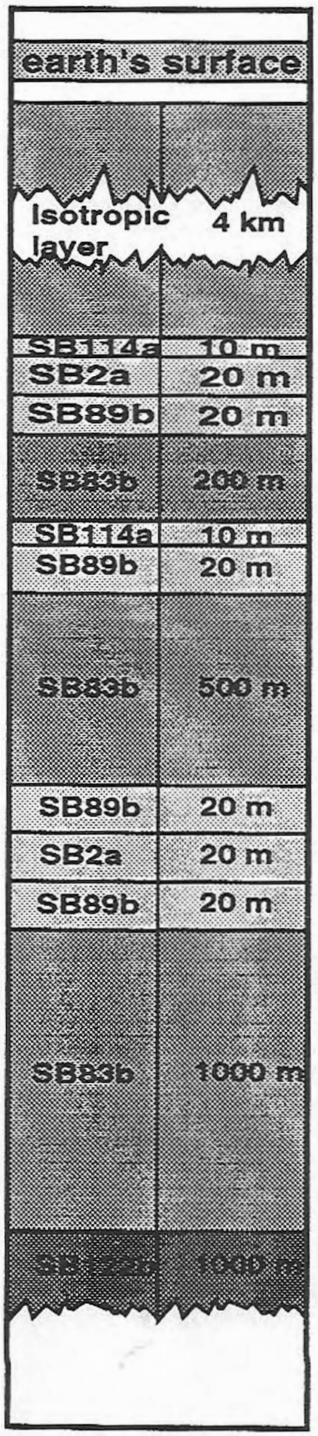

Fig. 11. *1D geological model, composed by a succession of the five samples studied. The relative thicknesses are not drawn to scale. The left column indicates the sample name and the thickness is in the right column.*

Geometry of the model – seismic parameters

We have considered the St Barthélémy section at the end of the period of extension, under upper crustal conditions (about 4 km depth), with the structures horizontal. The model was composed of 13 layers (Fig. 11). The anastomosing character of the shear zone is represented by three repeated sequences of mylonites separated by a layer of gneiss several hundred metres in thickness. Each mylonite layer was 10 or 20 metres thick. This very simple approach is clearly not a true 3D seismic modelling. Layers are indeed planes, horizontal and laterally homogeneous. Only the seismic velocities have three dimensional variations. The corresponding isotropic modelling using the average elastic parameters has not been carried out because the main interest of such a model is to study the first-order seismic signature it can generate rather than the influence of anisotropy.

The characteristics of the seismic line were as follows: the source was omnidirectional with a ricker centred at 30 Hz situated at one end of the seismic line on surface. 80 receivers were aligned in a parallel array every 100 metres. The rock layers were plane and horizontal. The calculated seismic signatures are P–P and P–S reflections on each interface.

Results

On seismic traces (Fig. 12) vertical movements display well the three P wave reflections generated by the three shear zones, between 1.3 and 1.6 s. The contact gneiss/granulites also generates a strong P reflection (at about 2 s). The first P–S reflections are also visible at about 1.7 s but have a smaller amplitude. On the radial movement traces, P-wave reflections become visible at about 1.5 km offset (at about 1.3 s) and their small amplitudes increase with increasing offset whereas P–S reflections have a stronger amplitude and are visible even at small offsets (0.5 km and 1.7 s).

CONCLUSIONS

In this study, the seismic properties of a ductile shear zone have been studied. Whereas the rock types have been represented by a small number of samples (5), the results provide much information and show the usefulness of the methods.

The seismic properties have been determined using different but complementary methods. Each one has its own advantages: (i) Laboratory measurements give direct and accurate control of seismic properties, in an important range of geological conditions (pressures up to 600 MPa and temperatures up to 600°C). In addition to the classic P-wave velocity measurement we have also measured the S-waves (velocities, polarization planes and bi-

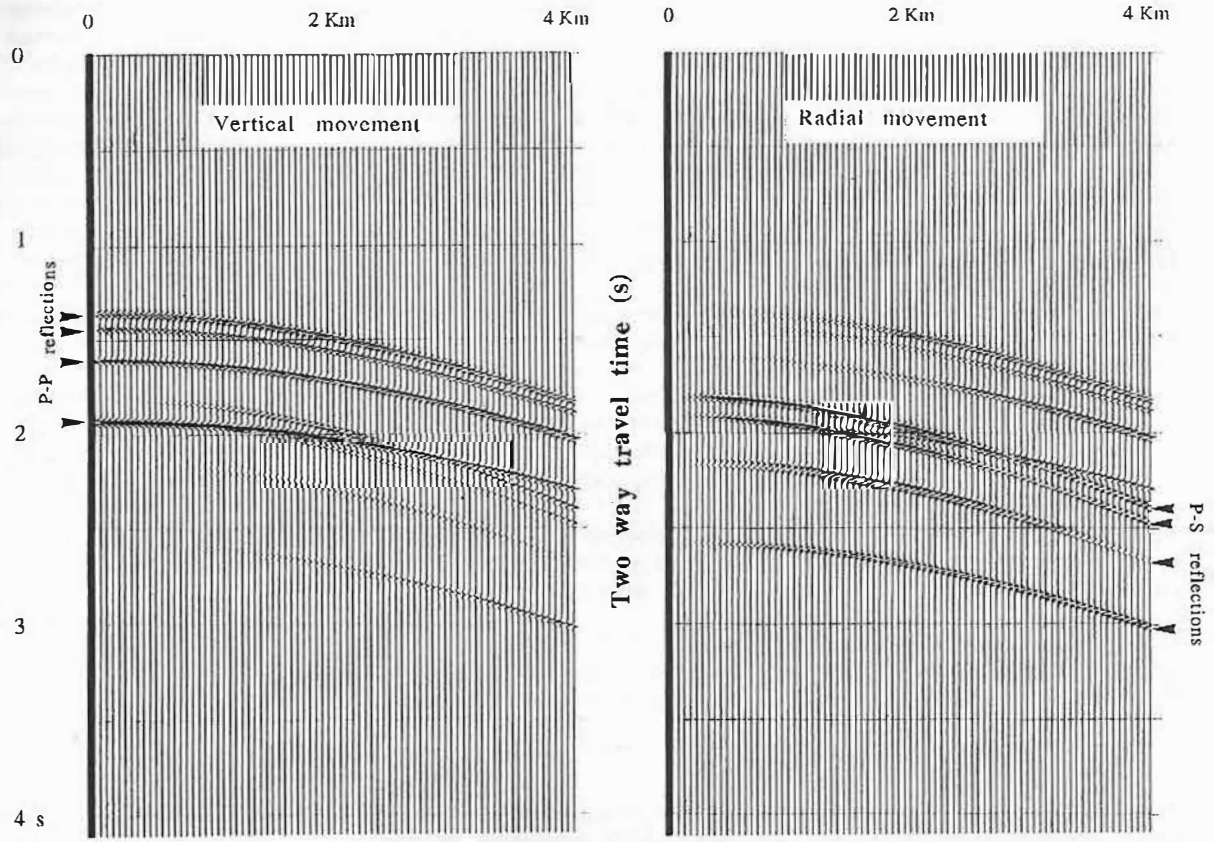

Fig. 12. *Seismic traces corresponding to the model shown in Fig. 12. The vertical movements and the radial movement are displayed, respectively on the left and on the right.*

refringence) which are an important seismic and kinematic diagnostic. (ii) The calculation of the elastic properties from petrofabric data allows the determination of the true 3D variations of the complete seismic properties (characterized by the 21 elastic constants). An interesting approach, shown here, is to study the respective influence of each mineral phase on the seismic properties of the aggregate as a whole. The knowledge of petrofabrics has also a structural and kinematic interest.

Petrofabrics have been determined using different and complementary tools: (i) Optical microscopy allows the determination of LPO of simple mineral phases (orthorhombic crystal symmetry for example). (ii) Neutron diffraction goniometry gives a very good representative LPO of a single phased rock and (iii) SEM is a powerful tool for the study of complex aggregates of low symmetry mineral phases (trigonal, monoclinic or triclinic for example).

The results measured (in laboratory) and calculated (from petrofabrics) for the two samples on which the two methods have been applied (SB114A and SB83b), are in good agreement.

The seismic modelling shows that such a schematic representation of a geological structure may generate reflections looking like those commonly observed on seismic profiles.

Finally, the main potential value of 3D seismic anisotropy is the extraction of the kinematic information carried by shear waves. Real, three component seismic records of S-wave polarization planes and of S-wave splitting may provide structural and kinematic information (Silver and Chan, 1988). This study has shown how one may determine the three dimensional shear wave properties (velocities, polarization planes, birefringence) of complex rocks. The 3D synthetic seismogram and the 3 component recording give us the opportunity to model the shear wave splitting.

ACKNOWLEDGEMENTS

This study has been supported by the Accompagnement ECORS 89/90 program. Thanks to G. Lloyd for the useful help and advice for the SEM measurements undertaken at Leeds University (England), to E. Rutter and K.J. Sandmeier for their constructive comments, to the C.E.A. (Saclay) for the neutron diffraction measurements kindly undertaken by T. Baudin, to the Compagnie Générale de Géophysique (Massy) for the program for 3D seismic modelling, to the Centre National Universitaire Sud de Calcul (Montpellier) for the computation time on the IBM 3090.

REFERENCES

Aleksandrov K.S., Alchikov U.V., Belikov B.P., Zaslavskii B.I. and Krupnyi A.I. (1974) Velocities of elastic waves in minerals at atmospheric pressure and increasing precision of elastic constants by means of EVM (in Russian), *Izv. Acad. Sci. USSR, Geol. Ser.*, **10**, 15–24.

Aleksandrov K.S. and Ryzhova T.V. (1961) The elastic properties of rock forming minerals, II: Layered silicates, *Izv. Acad. Sci. USSR, Geophys. Phys. Solid Earth*, 1165–1168.

Allard B. and Sotin C. (1988) Determination of mineral phase percentages in granular rocks by image analysis on a microcomputer, *Computer & Geosciences*, **14**, 261–269.

Barruol G. (1988) Anisotropies sismiques dans la croûte inférieure. Exemple de la section du Val Sesia dans la Zone d'Ivrée, *D.E.A.*, Montpellier II, 122 pp.

Choukroune P. and Pyrénées ECORS Team (1989) The ECORS Pyrenean deep seismic profile reflection data and the overall structure of an orogenic belt, *Tectonics*, **8**, 23–39.

Christensen N.I. (1979) Compressional wave velocities in rocks at high temperatures and pressures, critical thermal gradient, and crustal low-velocity zones, *J. geophys. Res.*, **84**, 6849–6857.

Christensen N.I. and Crosson R.S. (1968) Seismic anisotropy in the upper mantle, *Tectonophys.*, **6**, 93–107.

Christensen N.I. and Szymanski D.L. (1988) Origin of reflections from the Brevard fault zone, *J. geophys. Res.*, **93**, 1087–1102.

Cook F.A., Albaugh D.S., Brown L.D. and Hatcher R.D. (1979) Thin-skinned tectonics in the crystalline southern Appalachians; COCORP seismic reflection profiling of the Blue Ridge and Piedmont, *Geology*, **7**, 563–567.

Crampin S. (1985) Evaluation of anisotropy by shear-wave splitting, *Geophysics*, **50**, 142–152.

Crosson R.S. and Lin J.W. (1971) Voigt and Reuss prediction of anisotropic elasticity of dunite, *J. geophys. Res.*, **76**, 570–578.

Fountain D.M., Hurich C.A. and Smithson S.B. (1984) Seismic reflectivity of mylonite zones in the crust, *Geology*, **12**, 195–198.

Jones T.D. and Nur A. (1984) The nature of seismic reflection from deep crustal fault zone, *J. geophys. Res.*, **89**, 3153–3171.

Kern H. (1982) Elastic-wave velocity in crustal and mantle rocks at high pressure and temperature: the role of the high-low quartz transition and of dehydration reactions, *Phys. Earth Planet. Int.*, **29**, 12–23.

Kern H. (1990) Laboratory seismic measurements: an aid in the interpretation of seismic field data, *Terra Nova*, **2**, 617–628.

Kern H. and Richter A. (1981) Temperature derivatives of compressional and shear wave velocities in crustal and mantle rocks at 6 Kbar confining pressure, *J. Geophys.*, **49**, 47–56.

Kern H. and Schenk V. (1988) A model of velocity structure beneath Calabria, southern Italy, based on laboratory data, *Earth Planet. Sci. Letts*, **87**, 325–337.

Kern H. and Wenk H.R. (1990) Fabric-related velocity anisotropy and shear wave splitting in rocks from Santa Rosa mylonite zone, California, *J. geophys. Res.*, **95**, 11213–11223.

Lloyd G.E., Cockayne B. and Jones D.W. (1981) Selected-area electron channelling patterns from geological materials: specimen preparation and representation of patterns and applications, *Can. Miner.*, **19**, 505–518.

Lloyd G.E., Ferguson C.C. and Law R.D. (1987) Discriminatory petrofabric analysis of quartz rocks using SEM electron channelling, *Tectonophys.*, **135**, 243–249.

Mainprice D. (1990) A FORTRAN program to calculate seismic anisotropy from the lattice preferred orientation of minerals, *Computers & Geosciences*, **16**, 385–393.

Mainprice D., Casey M. and Schmid S. (1990) The seismic properties of alpine quartz mylonites determined from the orientation distribution functions, *Mem. Soc. géol. Fr.*, **156**, 85–95.

Mainprice D. and Nicolas A. (1989) Development of shape and lattice preferred orientations: applications to the seismic anisotropy of the lower crust, *J. Struct. Geol.*, **11**, 175–189.

McDonough D.T. and Fountain D.M. (1968) Reflection characteristics of a mylonite zone based on compressional waves velocities of rock samples, *Geophys. J.*, **93**, 547–558.

McSkimin H.J., Anreatch J.R. and Thurston R.N. (1965) Elastic moduli of quartz versus hydrostatic pressure at 25° and −195.8°C, *J. Appl. Phys.*, **36**, 1624–1632.

Nicolas A., Polino R., Hirn A. and Nicolich R. (1990) ECORS–CROP traverse and the deep structure of the western Alps: a synthesis, *Mém. Soc. géol. France*, **156**, 15–27.

Passchier C.W. (1982) Mylonitic deformation in the St-Barthélémy massif, French Pyrénées, with emphasis on the generation relationship between ultramylonite and pseudotachylite, *A.G.U. Pap. Geol.*, **1 (16)**, 1–173.

Peselnick L., Nicolas A. and Stevenson P.R. (1974) Velocity anisotropy in a mantle peridotite from the Ivrea Zone: Application to upper mantle anisotropy, *J. geophys. Res.*, **79**, 1175–1182.

Saint Blanquat M. (1989) La faille normale du massif du Saint Barthélémy. Age et signification de l'extension crustale dans la zone Nord Pyrénéenne, Doctorat, Montpellier II, 272 pp.

Saint Blanquat M. (1990) Petrological argument for high temperature extensional deformation in the Pyrenean Variscan crust (Saint Barthélémy Massif, Ariège, France), *Tectonophys.*, **177**, 245–262.

Schmid S.M. and Casey M. (1986) Complete fabric analysis of some commonly observed quartz c-axis patterns, In: *Paterson Volume* (ed. by H.C. Heard and B.E. Hobbs), pp. 263–286. AGU Monogr., Washington.

Schmidt N.H. and Olsen N.O. (1989) Computer-aided determination of crystal-lattic orientation from electron-chanelling patterns in the SEM, *Can. Miner.*, **27**, 15–22.

Seront B., Mainprice D. and Christensen N.I. (1992) A determination of the 3-dimensional seismic properties of an anorthosite – Comparison between values calculated from petrofabric and direct laboratory measurements, *J. geophys. Res.*, submitted.

Silver P.G. and Chan W. (1988) Implications for continental structure and evolution from seismic anisotropy, *Nature*, **335**, 34–39.

Vaughan M.T. and Guggenheim S. (1986) Elasticity of muscovite and its relationship to crystal structure, *J. geophys. Res.*, **91**, 4657–4664.